Supplementary Materials for

The global carbon balance of forests based on flux towers and forest age data

Ciais *et al.*

1. Global forest age map and sampling of age distribution by flux towers

a

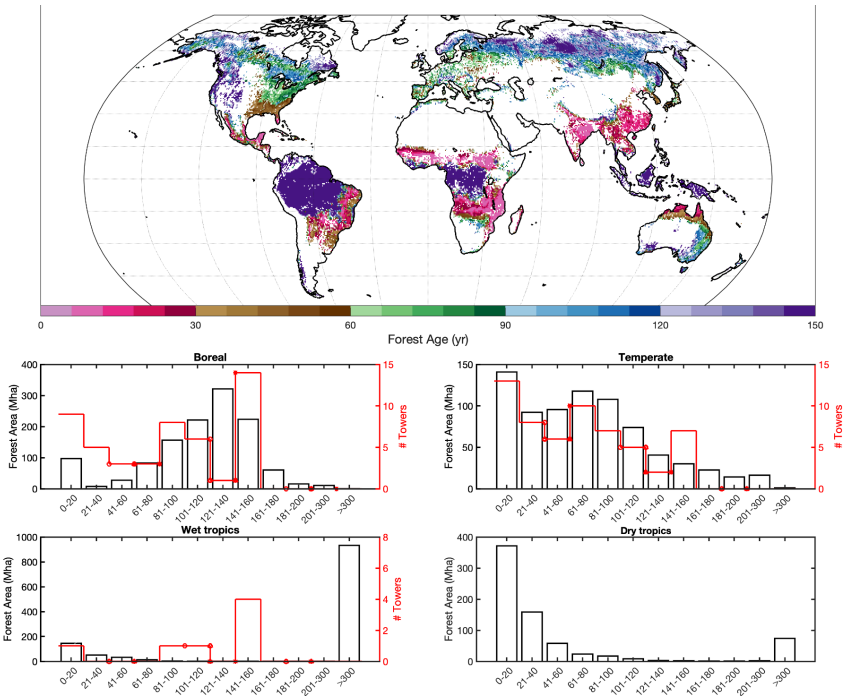

b

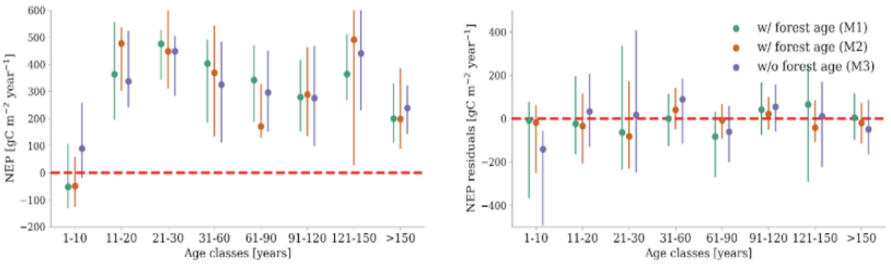

Figure S1. **a.** Forest age distribution for four biomes derived from the forest age map of Besnard et al. [1] used to upscale NEP. In red is the sampling of forest age by flux towers. **b.** Prediction of NEP from random forest models M1, M2 and M3 across all sites for different age bins, showing that models M1 and M2, which include age as a covariate, properly capture the negative NEP values indicating a carbon loss in young ages (0-10 years-old) unlike model M3 which only includes GPP, nitrogen deposition and

temperature. **c.** Residual of random forest models vs site observed NEP (observed minus modeled values) showing that model M3 over-estimates carbon sinks in young forests (0-10 years old). All flux tower data and their annual NEP are given in Table S1.

2. Regional NEP-age curves from chronosequences in temperate and boreal forests

For building the chronosequence regional NEP-age curves used in model M1, we searched the scientific literature for temperate and boreal forest NEP observations that measured chronosequences (different age cohorts after stand-replacing disturbances) in a given small region. We included only studies where measurements include young and old forests in the same region. When studies measured too few sites, we searched for other studies containing nearby forest measurements to complete the NEP-age chronosequence curves. The data sources and publication references are presented in Table S2.

In total, we were able to build seven NEP-age curves for the evergreen needleleaf forests (ENF) and deciduous broadleaf forests (DBF) biomes in temperate and boreal regions (see biomes definition in section 3). NEP-age data was collected by three methods: direct measurement of NEP by eddy covariance with multiple flux towers installed over stands of different ages in the same small region (EC in Table S1), biometric measurement of NPP with chamber-based measurement of soil heterotrophic respiration (biometric in Table S2), and time-derivative of biometric measurements of total ecosystem carbon stocks at different ages including vegetation and soil (Δ Stock in Table S2). The curves are displayed in Figure 1 of the main text and Figure S2.

In North America, four curves for boreal ENF forests used exclusively eddy covariance measurements (C1, C2 in Figure S2), one for temperate ENF forests used EC measurements (C3), one for temperate DBF forest (C7) used a combination of eddy-covariance and biometric measurements (Table S2). In Europe, one curve (C3) is for boreal ENF forests and one for temperate DBF forests (C6), both based on eddy-covariance measurements (Table S2). In Siberia, one curve was built for ENF forests (C4) using time derivatives of intensive biomass and soil C stock measurements across multiple ages since fire disturbance (Table S2).

We used least-squares non-linear regression to fit NEP-age curves for each chrono-sequence following the function proposed by Tang et al. [2] (equation 1). The fit parameter values are given in Table S3.

$$NEP(t) = k_0 \times t^{k1} \times e^{k_2 \times t} - k_3 \qquad (1)$$

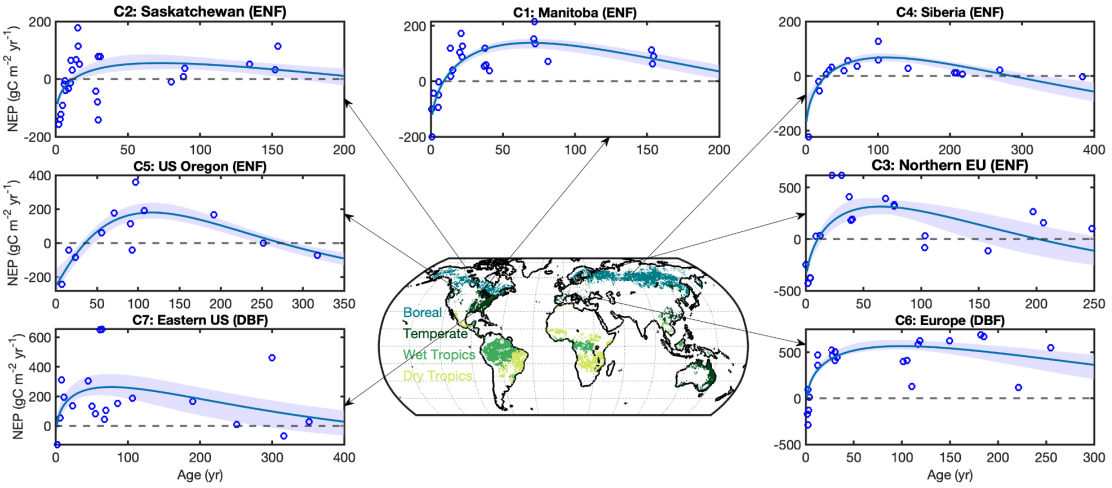

Figure S2 Regional NEP-age curves for temperate and boreal regions. The circles are site observations, and the solid line is the best-fit estimate with shaded areas showing the standard deviations of 18 fits obtained by bootstrapping the data.

Figure S3 shows the global NEP-age curve for model M2 fitted to all flux towers using the Amiro et al. [3] function.

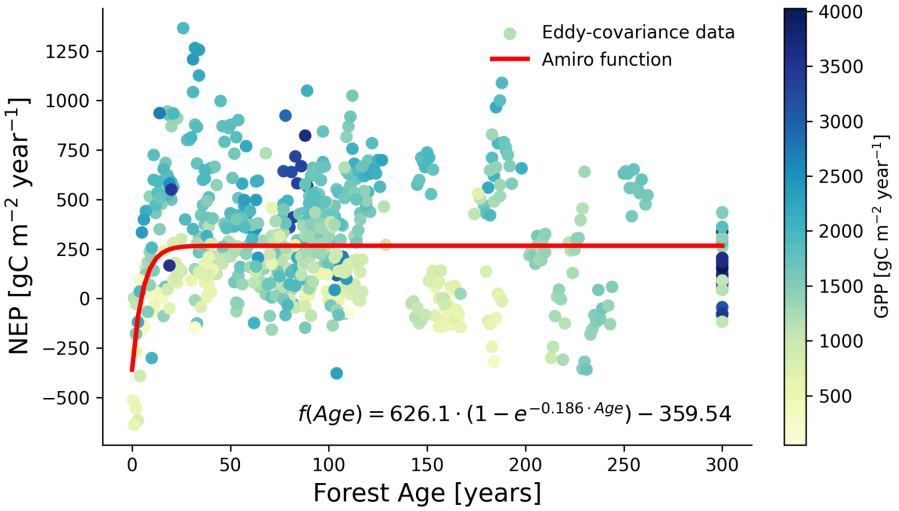

Figure S3 Global NEP-age curve fitted directly using all flux tower data fitted by the Amiro et al. [3] function. Each tower NEP - age point is coloured by its annual GPP.

3. Regional NEP-age curves from chronosequences in tropical forests

There are no eddy-covariance-based forest chronosequence NEP observations available in the Tropics. On the other hand, plot-level forest aboveground biomass changes at

multiple ages are relatively abundant [4–6], and wood decay dynamics after logging or forest clearing [7]. We, therefore, used the time derivative of carbon stock across multiple ages to infer NEP as a function of age (Δstock method in Table S2). We used an exponential equation to fit the growth of aboveground biomass with increasing age *(t)* after disturbance.

$$B(t) = B_{max} \times \left(1 - e^{-k_1 t}\right) \quad (2)$$

Where B_{max} is the asymptotic maximum above-ground biomass obtained from old-growth forest values. For decaying coarse woody debris (CWD), we used the equation:

$$CWD(t) = CWD_{max} \times \left(1 - e^{-k_2 t}\right) \quad (3)$$

Where CWD_{max} is the initial woody debris mass after a disturbance, assumed to be equal to the asymptotic maximum aboveground biomass B_{max}, and k_2 *is* a decay constant. Unlike boreal forests, which are subject to stand-replacing fire events and where post-fire soil C increases with time [8], soil carbon in tropical forests shows no large changes with time and changes of soil carbon were ignored in the total carbon stock change [9,10] and NEP. Belowground biomass and dead roots decay over time components were excluded from the calculation NEP. In other words, we assumed that AGB and CWD changes dominate tropical forest NEP-age curves over time. The time derivative of *B(t) + CWD(t)* gives the NEP-age curve.

$$NEP(t) = \frac{dB}{dt} + \frac{d(CWD)}{dt} = B_{max} \times k_1 \times e^{-k_1 \times t} + CWD_{max} \times k_2 \times e^{-k_2 \times t} \quad (4)$$

By construction, the cumulative NEP integrated from age $t = 0$ to $t = +\infty$ is zero. We derived the values of B_{max} and k_1 using observations from a 25-ha plot of a tropical evergreen forest in French Guiana that was clear-cut in 1976, abandoned to regrowth without human intervention, and monitored regularly [11]. The asymptotic value of biomass B_{max} is taken from measurements of a nearby old-growth forest where inventory data are from plots covering 120 ha [11]. The value of $\boldsymbol{k_2}$ is determined by synthesizing decomposition rates of each wood log as simulated by the wood log decomposition model of ref. [7] using forest inventory information from several forest plots in Costa Rica and French Guiana [12,13]. From these procedures, k_1 is derived as 0.0198 yr^{-1} with a standard error of 0.0017, and k_2 is fitted as 0.0666 yr^{-1} with a standard error of 0.0116.

The values of k_1 and k_2 derived from data in French Guiana were used for all tropical wet forests. Still, to account for the regional differences in B_{max}, we split the tropical wet forest biome into seven sub-regions, as explained in section 4 (Figure S4). Regional B_{max} values are obtained from forest inventories and the biomass map of South America [6]. We calculated the mean value and standard deviation of B_{max} for each region. Measurements for Africa, Asia & Oceania are from the website of the Forest Observation System (http://forest-observation-system.net/), now included in the GEO-TREES database (https://data.geo-trees.org/). We excluded measurements that are low outliers or represent dry forest or woodland. B_{max} values of wet tropical forest sub-regions and their standard deviations are given in Table S4.

For tropical dry forests, we used a Michaelis-Menten curve to fit the aboveground biomass growth with age, using the data from Poorter et al. [5] for South America. For Africa, biometric measurements of AGB time series were collected from McNicol et al. [15], Kalaba et al. [16], and Williams et al. [14]. We then assumed that CWD is a certain percentage of B_{max} and continues to decompose as the forest regrows. The first-order differential carbon stock curve was derived, providing the NEP-age relationship for tropical dry forests (Figure 2). The resulting NEP likely overestimates the NEP sink after disturbance because it ignores CO_2 emissions from soil organic carbon's decay and charred tree material's decomposition.

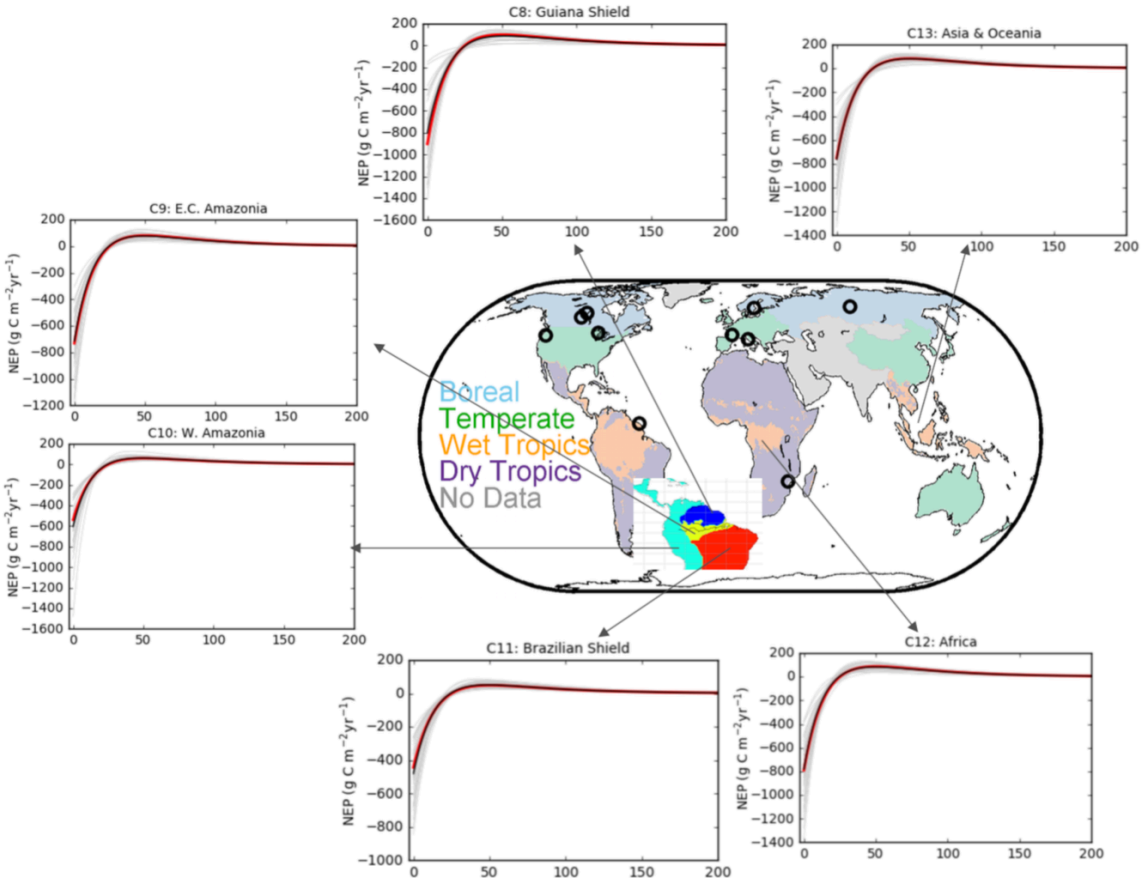

Figure S4 Regional NEP-age curves for tropical wet forests obtained by taking the time derivative of AGB and CWD stocks to obtain NEP as a function of age since a stand-replacing disturbance.

4. Decision tree to assign a biome-specific NEP-age curve to each grid cell

Each 0.5° grid cell (x) belonging to a biome (b) is assigned an empirical NEP-age curve denoted $f^{b}(age_{x\in b})$ in the Methods section. We used a hierarchical decision tree illustrated in Figure S5 to assign to each grid cell a unique biome and a unique NEP-age curve from the curves defined in the previous sections. To assign a biome to each grid cell, all forested grid cells are first classified into the boreal, temperate and tropical forests classes as defined by Pan et al. [17]. The tropics are further divided into wet and dry forests based on the consensus land cover map of ref. [18]. Their *evergreen broadleaf* class in the tropics define the wet forests, and the *deciduous broadleaf trees* and *mixed/other trees* are the dry forests. The relative fractions of wet versus dry forests were then calculated for each grid cell. A grid cell with a > 50% wet forest cover was considered in the wet tropical forest biome and vice-versa for dry forests. Temperate and boreal forests

from Pan et al. [17] were further subdivided into Evergreen Needle-leaf (ENF) and Deciduous Broadleaf (DBF) forests using the classification of Tuanmu et al. [18] Needle-leaf deciduous (NDF) forests were grouped with ENF, and evergreen broadleaf (EBF) with DBF (Figure S5). The seven different NEP-age curves (C1-C7) obtained from regional chronosequences in temperate and boreal forests (Figure S2) were finally assigned to the DBF or ENF biome, with a further distinction per continent (Figure S5). In the wet tropics, we considered six sub-regions differentiated by their maximum AGB to define the NEP-age curves: Africa, Asia and Oceania, the Guiana Shield, Eastern and Central Amazonia, Western Amazonia and the Brazilian Shield. Our more detailed subdivision of the Amazon wet forests into subregions accounts for spatial gradients in maximum AGB, mainly related to soil fertility and tree growth rates [6].

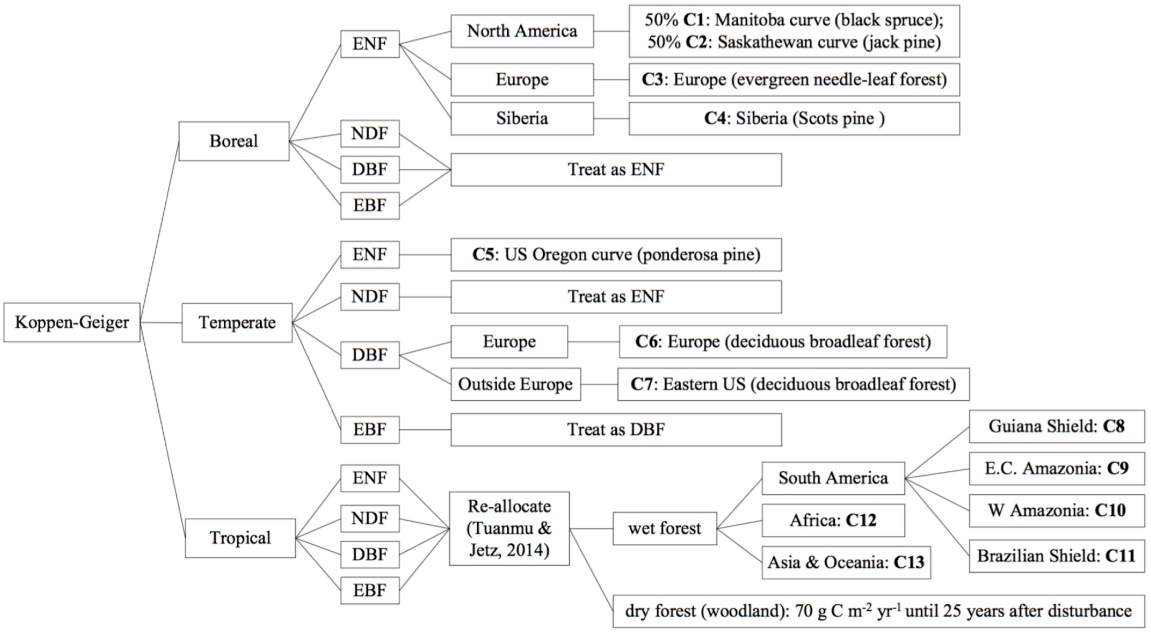

Figure S5 Classification associating each 0.5° pixel with a NEP-age curve corresponding to a biome. There are, in total, 13 regional NEP-age curves, as "C1" to "C13" in figure S2. ENF: Evergreen Needle-leaf Forest; NDF: Needleleaf Deciduous Forest; DBF: Deciduous Broadleaf Forest; and EBF: Evergreen Broadleaf Forests (Figures S2 and S3).

5. Models used for upscaling NEP predictions from sites to global 0.5° maps and uncertainties on NEP maps

Random forest algorithms

The Random Forest (RF) models used in this study are a diagnostic non-parametric ensemble modelling technique that can construct an ensemble of decision trees that vote on predictions [19]. This algorithm integrates multiple independent variables without relying on their statistical distribution or covariance structure. Bootstrap samples are used to construct multiple trees, and each tree is grown with a randomized selection of predictors to maintain a low bias [20]. Its ensemble attributes can help achieve higher prediction accuracies than traditional regression trees. Some recent studies have also demonstrated RF's utility in predicting carbon fluxes [21–23].

Aleatoric uncertainty of gridded NEP maps (data uncertainty)

To calculate the aleatoric uncertainty (related to the data uncertainty) of gridded NEP maps obtained with the RF model in the M1 approach, we performed an ensemble of simulations using perturbed NEP-age curves (see below), nine gridded GPP fields from ref. [24], one gridded mean annual temperature field and 20 forest age fields from the GAMIv2.0 product [25]. Uncertainties on the temperate and boreal biomes NEP-age curves are derived from bootstrapping data used in the fits from Equations (1) and (4). Uncertainties on NEP-age curves for tropical wet forests are constructed by sampling nine k_1, k_2 and B_{max} values using their mean values and standard deviations assuming a normal distribution, with B_{max} data from Table S4. Uncertainties of up-scaled NEP in the M2 approach were derived from 9 members of the global NEP-age curve (Figure S3) obtained by varying the parameters of the Amiro et al. [3] equation used by ref. [26]. A bootstrapping algorithm was used to create an ensemble of 500 random re-samplings of the model parameters from which nine sets of parameters were randomly sampled.

Epistemic uncertainty of gridded NEP maps (model uncertainty)

The epistemic uncertainty (related to the RF model itself) is estimated using a quantile random forest applied to each ensemble model. This algorithm provides an output of all the deciles of the NEP distribution in each grid cell, from which we estimate the aleatoric uncertainty in each grid cell using a bootstrap method, randomly sampling each decile and each member.

The total uncertainty of NEP maps

The final uncertainty is obtained by adding the data and model uncertainties using a Monte Carlo method to sample their distributions, which are assumed to be independent.

For biome mean NEP uncertainties (Table 1 in the main text) we calculated the mean of all grid cells belonging to each biome and then the final uncertainty as explained above. Uncertainties are reported as Mean Absolute Deviation in the main text; uncertainties calculated as an interquartile range give similar results (Table S4 shows interquartile instead of standard deviations used in Table 1 in the main text).

Source and sink areas

Figure S6 shows the area with NEP sources and sinks from the three upscaling models. Model M1 has larger source areas in northern boreal forests (reflecting very young ages from fires, the NEP age curves of Fig S2, and GPP and climate predictors). Model M3 also has several source areas in this region, caused by climate and GPP conditions.

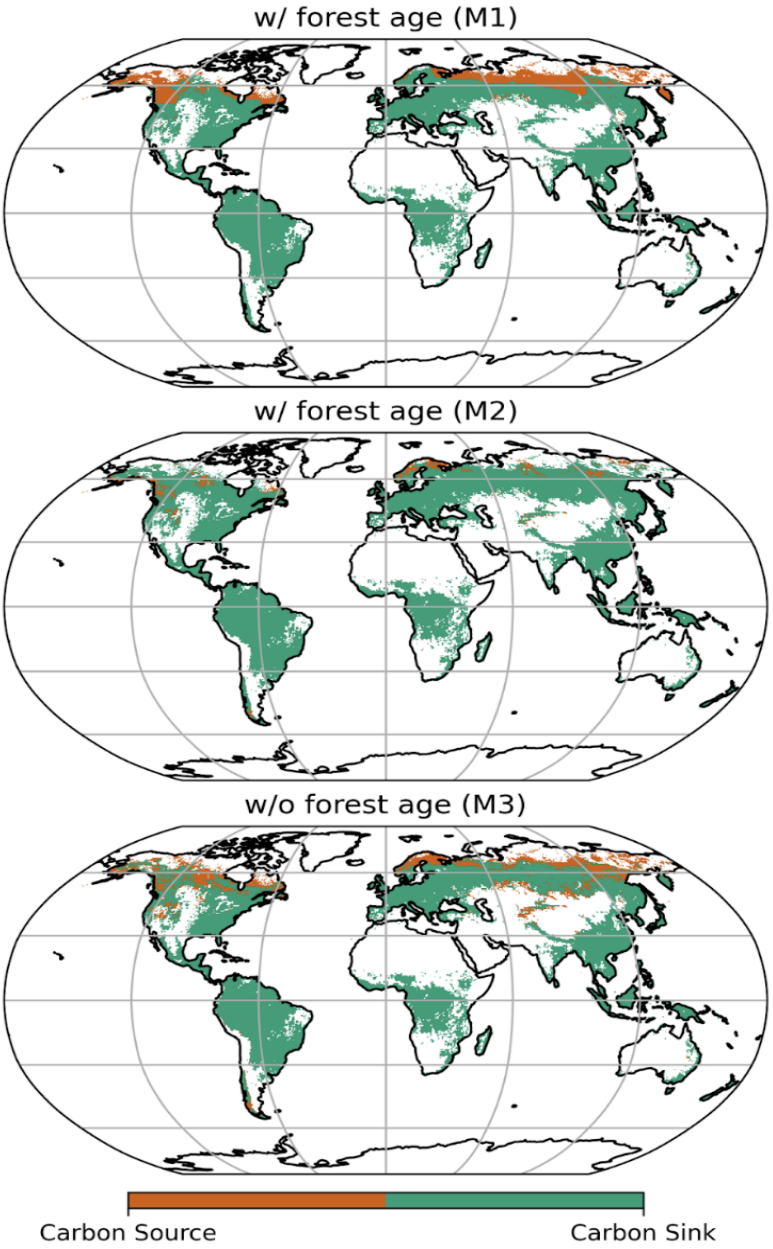

Figure S6. Areas with NEP sources and sinks from the three upscaling models.

6. Cross-validation of random forest models trained at the site level

Evaluation of predicted NEP against flux tower sites used as cross-validation

For evaluating predicted site-level NEP by the random forests models, we used a leave-one-out cross-validation (LOOCV) technique. LOOCV ensures the independence between the training and validating samples and greatly alleviates the overfitting problem [21]. All sites in our NEP dataset of 119 sites are sequentially excluded from the training set

and used for validation purposes. When a site is excluded, all measurements for different years at this site are excluded. The result of LOOCV is presented in Figure S7.

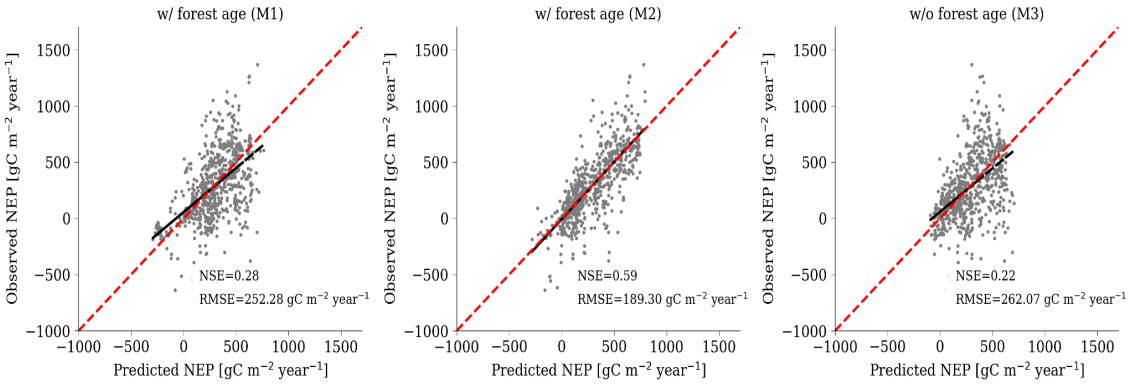

Figure S7. Cross-validation results were obtained using a leave-one flux tower out for the M1, M2, and M3 random forest models.

Proof of no age-dependent bias in predicted NEP across all training sites

We examined the age dependence of the bias between predicted and observed site NEP to verify whether the forest age effect is fully taken into account in our models. Figure S1b shows the predicted NEP and the residuals of observed minus predicted NEP for different age bins. Figure S8 shows the residuals for different age bins at each site, for different biomes and GPP. The data in this figure show no systematic age dependency of the residuals of the fit of NEP vs age, suggesting that the modeled estimate of NEP is not biased in certain age classes. Note that the M2 method has less scatter of residuals in the range 40-100 years old.

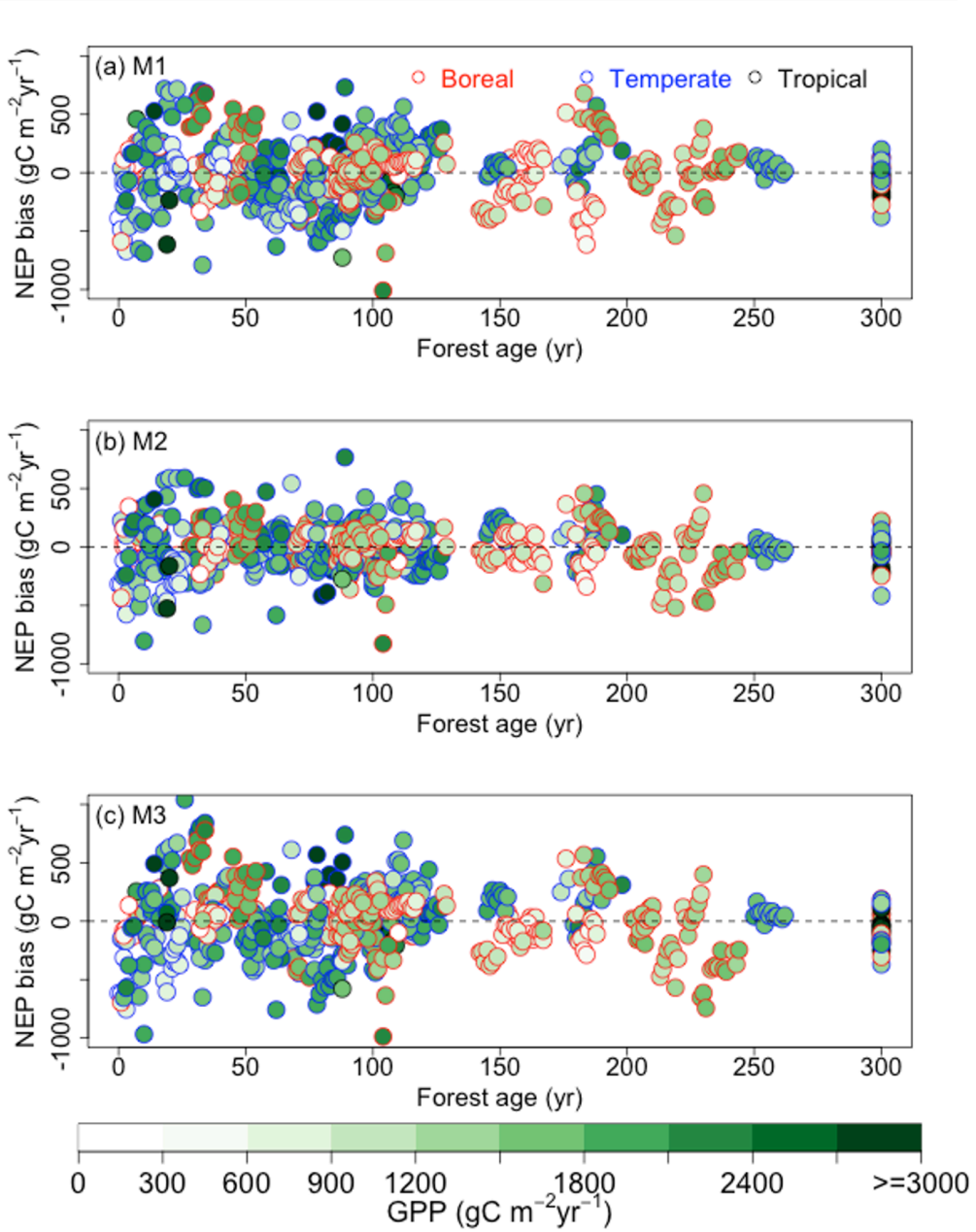

Figure S8. Dependency of the NEP-age fit residuals (simulated NEP with random forest models minus site observed NEP) as a function of age, with the color of each site being GPP. No obvious bias was found as a function of age, showing that the models capture the shape of NEP with age shown in Fig S1b.

8. Comparison of the northern vs tropical carbon sink distribution with inversions

Using established forest NBP results from Table 1 in the main text, aggregated for wet and dry tropics into the Tropics and for boreal and temperate into the northern hemisphere, we

took the mean of the M1 and M2 NBP model results. We added gross deforestation losses from the average of ref. [27] and ref. [28] as these losses were not included in our models restricted to NBP over established forests, including regrowing forests. We used inversion data from the TRANSCOM3 ensemble used by Stephens et al. [29] constrained by vertical CO_2 profiles, and a more recent inversion ensemble used by Gaubert et al. [30] constrained by CO_2 vertical profiles from the large-scale HIPPO atmospheric campaign. The results are shown in Table S5 for both inversion ensembles.

NEP-age Curve No.	Age (year)	NEP g C m^{-2} yr^{-1}	Method	Latitude	Longitude	Species	Source
C1	153	110	EC	55.9	-98.4	Spruce	Amiro et al. 2011
C1	154	65	EC	55.9	-98.4	Spruce	Amiro et al. 2011
C1	155	90	EC	55.9	-98.4	Spruce	Amiro et al. 2011
C1	72	154	EC	55.9	-98.4	Spruce	Amiro et al. 2011
C1	73	214	EC	55.9	-98.4	Spruce	Amiro et al. 2011
C1	74	136	EC	55.9	-98.4	Spruce	Amiro et al. 2011
C1	38	57	EC	55.9	-98.4	Spruce	Amiro et al. 2011
C1	39	120	EC	55.9	-98.4	Spruce	Amiro et al. 2011
C1	40	58	EC	55.9	-98.4	Spruce	Amiro et al. 2011
C1	41	41	EC	55.9	-98.4	Spruce	Amiro et al. 2011
C1	21	106	EC	55.9	-98.4	Spruce	Amiro et al. 2011
C1	22	168	EC	55.9	-98.4	Spruce	Amiro et al. 2011
C1	23	88	EC	55.9	-98.4	Spruce	Amiro et al. 2011
C1	24	125	EC	55.9	-98.4	Spruce	Amiro et al. 2011
C1	14	29	EC	55.9	-98.4	Spruce	Amiro et al. 2011
C1	15	22	EC	55.9	-98.4	Spruce	Amiro et al. 2011
C1	16	39	EC	55.9	-98.4	Spruce	Amiro et al. 2011
C1	5	-90	EC	55.9	-98.4	Spruce	Amiro et al. 2011
C1	6	-46	EC	55.9	-98.4	Spruce	Amiro et al. 2011
C1	7	-6	EC	55.9	-98.4	Spruce	Amiro et al. 2011
C1	1	-192	EC	55.9	-98.4	Spruce	Amiro et al. 2011
C1	2	-93	EC	55.9	-98.4	Spruce	Amiro et al. 2011
C1	82	70	EC	63.9	-145.4	Spruce	Amiro et al. 2011
C1	15	114	EC	63.9	-145.4	Spruce	Amiro et al. 2011
C1	3	-41	EC	63.9	-145.4	Spruce	Amiro et al. 2011

C2	27	-39	EC	54.5	-105.8	Jackpine	Amiro et al. 2011
C2	28	-78	EC	54.5	-105.8	Jackpine	Amiro et al. 2011
C2	29	-136	EC	54.5	-105.8	Jackpine	Amiro et al. 2011
C2	13	68	EC	54.3	-105.9	Jackpine	Amiro et al. 2011
C2	14	177	EC	54.3	-105.9	Jackpine	Amiro et al. 2011
C2	15	115	EC	54.3	-105.9	Jackpine	Amiro et al. 2011
C2	16	53	EC	54.3	-105.9	Jackpine	Amiro et al. 2011
C2	3	-132	EC	54.3	-105.9	Jackpine	Amiro et al. 2011
C2	4	-87	EC	54.3	-105.9	Jackpine	Amiro et al. 2011
C2	5	-5	EC	54.3	-105.9	Jackpine	Amiro et al. 2011
C2	6	3	EC	54.3	-105.9	Jackpine	Amiro et al. 2011
C2	7	-43	EC	54.3	-105.9	Jackpine	Amiro et al. 2011
C2	8	-33	EC	54.3	-105.9	Jackpine	Amiro et al. 2011
C2	0	-170	EC	53.9	-104.6	Jackpine	Howard et al. 2004
C2	5	-30	EC	53.9	-104.7	Jackpine	Howard et al. 2004
C2	10	65	EC	53.9	-104.7	Jackpine	Howard et al. 2004
C2	29	75	EC	53.9	-104.6	Jackpine	Howard et al. 2004
C2	79	-10	EC	53.9	-104.7	Jackpine	Howard et al. 2004
C2	2	-155	EC	53.9	-104.6	Jackpine	Mkhabela et al. 2009
C2	3	-123	EC	53.9	-104.6	Jackpine	Mkhabela et al. 2009
C2	10	-7	EC	53.9	-104.7	Jackpine	Mkhabela et al. 2009
C2	11	34	EC	53.9	-104.7	Jackpine	Mkhabela et al. 2009
C2	29	80	EC	53.9	-104.6	Jackpine	Mkhabela et al. 2009
C2	30	79	EC	53.9	-104.6	Jackpine	Mkhabela et al. 2009
C2	88	4	EC	53.9	-104.7	Jackpine	Mkhabela et al. 2009
C2	89	36	EC	53.9	-104.7	Jackpine	Mkhabela et al. 2009
C2	152	28	EC	55.9	-98.5		FLUXCOM
C2	154	114	EC	55.9	-98.5		FLUXCOM
C2	134	51	EC	54.0	-105.1		FLUXCOM
C3	4	-386	EC	61.9	24.3	Scots pine	Kolari et al. 2004

C3	12	24	EC	61.9	24.3	Scots pine	Kolari et al. 2004
C3	40	185	EC	61.9	24.3	Scots pine	Kolari et al. 2004
C3	75	323	EC	61.9	24.3	Scots pine	Kolari et al. 2004
C3	0	-258	EC	60.1	17.5	Scots pine	Magnani et al. 2007
C3	36	403	EC	60.1	17.5	Scots pine	Magnani et al. 2007
C3	68	382	EC	60.1	17.5	Scots pine	Magnani et al. 2007
C3	103	9	EC	60.1	17.5	Scots pine	Magnani et al. 2007
C3	4	-400	EC	61.9	24.3	Scots pine	Magnani et al. 2007
C3	12	11	EC	61.9	24.3	Scots pine	Magnani et al. 2007
C3	39	169	EC	61.9	24.3	Scots pine	Magnani et al. 2007
C3	40	181	EC	61.9	24.3	Scots pine	Magnani et al. 2007
C3	75	311	EC	61.9	24.3	Scots pine	Magnani et al. 2007
C3	3	-444	EC	55.2	2.1	Picea sitchensis	Magnani et al. 2007
C3	8	13	EC	55.2	2.1	Picea sitchensis	Magnani et al. 2007
C3	21	620	EC	55.2	2.1	Picea sitchensis	Magnani et al. 2007
C3	30	620	EC	55.2	2.1	Picea sitchensis	Magnani et al. 2007
C3	157	-141	EC	56.5	32.9		FLUXCOM
C3	102	-103	EC	60.1	17.5		FLUXCOM
C3	197	265	EC				Luyssaert et al. 2008
C3	206	157	EC				Luyssaert et al. 2008
C3	248	100.6	EC				Luyssaert et al. 2008
C4	53	58	Δ Stock	60.7	89.1	Scots pine	Wirth et al. 2002
C4	95	56	Δ Stock	60.7	89.1	Scots pine	Wirth et al. 2002
C4	266	23	Δ Stock	60.7	89.1	Scots pine	Wirth et al. 2002
C4	2	-221	Δ Stock	60.7	89.1	Scots pine	Wirth et al. 2002
C4	14	-53	Δ Stock	60.7	89.1	Scots pine	Wirth et al. 2002
C4	28	18	Δ Stock	60.7	89.1	Scots pine	Wirth et al. 2002
C4	31	29	Δ Stock	60.7	89.1	Scots pine	Wirth et al. 2002
C4	95	130	Δ Stock	60.7	89.1	Scots pine	Wirth et al. 2002
C4	67	37	Δ Stock	60.7	89.1	Scots pine	Wirth et al. 2002

C4	138	26	Δ Stock	60.7	89.1	Scots pine	Wirth et al. 2002
C4	200	16	Δ Stock	60.7	89.1	Scots pine	Wirth et al. 2002
C4	204	16	Δ Stock	60.7	89.1	Scots pine	Wirth et al. 2002
C4	383	4	Δ Stock	60.7	89.1	Scots pine	Wirth et al. 2002
C4	14	-20	Δ Stock	60.7	89.1	Scots pine	Wirth et al. 2002
C4	26	8	Δ Stock	60.7	89.1	Scots pine	Wirth et al. 2002
C4	48	18	Δ Stock	60.7	89.1	Scots pine	Wirth et al. 2002
C4	215	10	Δ Stock	60.7	89.1	Scots pine	Wirth et al. 2002
C5	23	-83	Biometric	44.4	-121.6	ponderosa pine	Law et al. 2003
C5	9	-244	Biometric	44.5	-121.7	ponderosa pine	Law et al. 2003
C5	16	-44	Biometric	44.4	-121.6	ponderosa pine	Law et al. 2003
C5	69	177	Biometric	44.4	-121.6	ponderosa pine	Law et al. 2003
C5	56	60	Biometric	44.4	-121.6	ponderosa pine	Law et al. 2003
C5	89	117	Biometric	44.5	-121.6	ponderosa pine	Law et al. 2003
C5	106	190	Biometric	44.4	-121.7	ponderosa pine	Law et al. 2003
C5	93	-40	Biometric	44.5	-121.7	ponderosa pine	Law et al. 2003
C5	96	359	Biometric	44.5	-121.7	ponderosa pine	Law et al. 2003
C5	190	168	Biometric	44.5	-121.6	ponderosa pine	Law et al. 2003
C5	251	4	Biometric	44.5	-121.6	ponderosa pine	Law et al. 2003
C5	316	-67	Biometric	44.4	-121.6	ponderosa pine	Law et al. 2003
C6	0	-179	EC	42.4	11.6	Quercus cerris	Magnani et al. 2007
C6	2	86	EC	42.4	11.6	Quercus cerris	Magnani et al. 2007
C6	2	-143	EC	42.4	11.6	Quercus cerris	Magnani et al. 2007
C6	2	-3	EC	42.4	11.6	Quercus cerris	Magnani et al. 2007
C6	11	356	EC	42.4	11.6	Quercus cerris	Magnani et al. 2007
C6	12	470	EC	42.4	11.6	Quercus cerris	Magnani et al. 2007
C6	0	-299	EC	44.6	0.9	Pinus pinaster	Magnani et al. 2007
C6	27	521	EC	44.6	0.9	Pinus pinaster	Magnani et al. 2007
C6	28	464	EC	44.6	0.9	Pinus pinaster	Magnani et al. 2007
C6	29	506	EC	44.6	0.9	Pinus pinaster	Magnani et al. 2007

C6	30	412	EC	44.6	0.9	Pinus pinaster	Magnani et al. 2007
C6	31	449	EC	44.6	0.9	Pinus pinaster	Magnani et al. 2007
C6	222	123	EC	46.8	9.9		FLUXCOM
C6	184	698	EC	47.5	8.4		FLUXCOM
C6	103	404	EC	39.3	-0.3		FLUXCOM
C6	111	122	EC	39.9	-5.8		FLUXCOM
C6	150	632	EC	48.5	2.8		FLUXCOM
C6	186	669	EC	46.6	11.4		FLUXCOM
C6	106	409	EC	52.2	5.7		FLUXCOM
C6	257	556	EC	51.1	10.5		FLUXCOM
C6	118	596	EC	51.3	10.4		FLUXCOM
C6	119	625	EC	51.0	13.6		FLUXCOM
C6	115	826	EC	41.8	13.6		FLUXCOM
C7	65	655	EC	46.3	-91.2	BDF	Noormets et al. 2007
C7	63	648	EC	46.3	-91.2	BDF	Noormets et al. 2007
C7	12	195	EC	46.3	-91.2	BDF	Noormets et al. 2007
C7	8	313	EC	46.3	-91.2	BDF	Noormets et al. 2007
C7	3	-128	EC	46.3	-91.2	BDF	Noormets et al. 2007
C7	300	464	EC	46.2	-89.3	BDF	Desai et al. 2005
C7	70	110	EC	45.8	-90.1	BDF	Desai et al. 2005
C7	45	303	EC	41.6	-83.8	BDF	Noormets et al. 2008
C7	85	153	Biometric	45.6	-84.7	BDF	Gough et al. 2007
C7	68	45	Biometric	45.6	-84.7	BDF	Gough et al. 2007
C7	56	80	Biometric	45.6	-84.7	BDF	Gough et al. 2007
C7	50	130	Biometric	45.6	-84.7	BDF	Gough et al. 2007
C7	24	135	Biometric	45.6	-84.7	BDF	Gough et al. 2007
C7	6	55	Biometric	45.6	-84.7	BDF	Gough et al. 2007
C7	106	190	Biometric	44.4	-121.7	BDF	Law et al. 2003
C7	190	168	Biometric	44.5	-121.6	BDF	Law et al. 2003
C7	251	4	Biometric	44.5	-121.6	BDF	Law et al. 2003

C7	316	-67	Biometric	44.4	-121.6	BDF	Law et al. 2003
C7	351	27	EC	46.2	-89.3		FLUXCOM

Table S1. Data used for building NEP-age curves in temperate and boreal biomes.

Curve No.	k_0	k_1	k_2	k_3	References
C1	81.1	0.44	-0.0063	202	Amiro et al. [3]
C2	93.5	0.28	-0.0039	180	Amiro et al. [3]; Howard et al. [31]; Mkhabela et al. [32]; FLUXCOM
C3	140.9	0.54	-0.0083	454	Kolari et al. [33]; Magnani et al. [34]; Luyssaert et al. [35]; FLUXCOM
C4	65.0	0.41	-0.0037	231	Wirth et al. [36]
C5	7.3	1.09	-0.0093	254	Law et al. [37]
C6	306.7	0.29	-0.0029	309	Magnani et al. [34]; FLUXCOM
C7	128.2	0.34	-0.0045	138	Noormets et al. [38]; Desai et al. [39]; Noormets et al. [40]; Gough et al. [41]; Law et al. [37]; FLUXCOM

Table S2 Parameters of fitted NEP-age curves in temperate and boreal forests.

Region	Guiana Shield	Eastern & Central Amazonia	Western Amazonia	Brazilian Shield	Africa	Asia & Oceania
B_{max} Mg C ha^{-1}	199.0 (44.2)	161.4 (38.6)	118.9 (24.3)	97.8 (35.5)	174.4 (41.4)	165.9 (30.3)

Table S3 Maximum aboveground biomass B_{max} in tropical wet forests for different subregions, with standard deviations in parentheses. B_{max} is the parameter used for fitting equation (4).

	Net Ecosystem Productivity NEP			Net Carbon Balance NBP			NBP from biomass inventories
	M1 model	M2 model	M3 model	M1	M2	M3	Pan *et al.* [17]
Boreal	$0.6^{0.9}_{0.3}$	$0.7^{1.1}_{0.3}$	$0.6^{1.1}_{0.2}$	$-0.1^{0.2}_{-0.4}$	$0.0^{0.4}_{-0.4}$	$-0.1^{0.4}_{-0.5}$	0.5 ± 0.1
Temperate	$2.2^{2.7}_{1.7}$	$2.1^{2.6}_{1.6}$	$2.1^{2.6}_{1.6}$	$1.5^{2.0}_{1.0}$	$1.4^{1.9}_{0.9}$	$1.4^{1.9}_{0.9}$	0.8 ± 0.1
Tropics	$3.4^{4.4}_{2.3}$	$3.3^{4.4}_{2.2}$	$3.1^{4.0}_{2.1}$	$1.6^{2.7}_{0.5}$	$1.6^{2.6}_{0.4}$	$1.3^{2.3}_{0.3}$	2.8 ± 0.7
Wet tropics	$1.7^{2.3}_{1.1}$	$1.8^{2.4}_{1.2}$	$1.8^{2.3}_{1.3}$	$0.7^{1.3}_{0.1}$	$0.8^{1.4}_{0.2}$	$0.8^{1.3}_{0.3}$	*N/A*
Dry tropics	$1.7^{2.2}_{1.2}$	$1.6^{2.0}_{1.0}$	$1.3^{1.7}_{0.8}$	$0.9^{1.3}_{0.3}$	$0.7^{1.2}_{0.2}$	$0.5^{0.9}_{0.0}$	*N/A*
Globe	$6.4^{8.3}_{4.5}$	$6.4^{8.5}_{4.2}$	$6.1^{8.1}_{4.1}$	$3.0^{4.9}_{1.1}$	$3.0^{5.1}_{0.9}$	$2.7^{4.7}_{0.7}$	4.1 ± 0.7

Table S4 NEP and NBP biome mean values in PgC year^{-1} with uncertainties calculated as the interquartile range of the data distribution and model-related uncertainties. The lower quartile is subscript, and the upper quartile is superscript.

	NBP of established forests	Gross deforestation emissions	Total NBP	Inversions	Inversions
	Average M1 and M2	Average Harris *et al.* [28] Houghton *et al.* [27]		Stephens *et al.*[29] (Transcom 3) consistent with aircraft vertical profiles of CO_2 (1992-1996)	Gaubert *et al.*[30] (RECCAP) consistent with HIPPO vertical profiles of CO_2 (2004-2014)
Northern	1.4 ± 0.8	0	1.4 ± 0.8	1.5 ± 0.6	2.2 ± 0.4
Tropics	1.6 ± 1.1	1.1 ± 0.5	0.5 ± 1.2	0.5 ± 0.8	0.1 ± 0.1
Globe	3.0 ± 2.0	1.1 ± 0.5	1.9 ± 2.1	2.0 ± 0.5	2.3 ± 0.5

Table S5. Our estimates of NBP compared to two inversion ensembles are constrained by atmospheric CO_2 profiles for partitioning CO_2 sinks between the northern hemisphere and the tropics.

References

1. Besnard, S. *et al.* Mapping global forest age from forest inventories, biomass and climate data. *Earth Syst. Sci. Data* **13**, 4881–4896 (2021).
2. Tang, J., Luyssaert, S., Richardson, A. D., Kutsch, W. & Janssens, I. A. Steeper declines in forest photosynthesis than respiration explain age-driven decreases in forest growth. *Proc. Natl. Acad. Sci. U. S. A.* **111**, 8856–8860 (2014).

3. Amiro, B. D. *et al.* Ecosystem carbon dioxide fluxes after disturbance in forests of North America. *J. Geophys. Res.* **115**, (2010).
4. Chazdon, R. L. *et al.* Carbon sequestration potential of second-growth forest regeneration in the Latin American tropics. *Sci. Adv.* **2**, e1501639 (2016).
5. Poorter, L. *et al.* Biomass resilience of Neotropical secondary forests. *Nature* **530**, 211–214 (2016).
6. Mitchard, E. T. A. *et al.* Markedly divergent estimates of Amazon forest carbon density from ground plots and satellites: Divergent forest carbon maps from plots & space. *Glob. Ecol. Biogeogr.* **23**, 935–946 (2014).
7. Hérault, B. *et al.* Modeling decay rates of dead wood in a neotropical forest. *Oecologia* **164**, 243–251 (2010).
8. Harden, J. W. *et al.* Spatiotemporal analysis of black spruce forest soils and implications for the fate of C. *J. Geophys. Res.* **117**, (2012).
9. Marín-Spiotta, E. & Sharma, S. Carbon storage in successional and plantation forest soils: a tropical analysis: Carbon in reforested and plantation soils. *Glob. Ecol. Biogeogr.* **22**, 105–117 (2013).
10. Schedlbauer, J. L. & Kavanagh, K. L. Soil carbon dynamics in a chronosequence of secondary forests in northeastern Costa Rica. *For. Ecol. Manage.* **255**, 1326–1335 (2008).
11. Chave, J. *et al.* Slow rate of secondary forest carbon accumulation in the Guianas compared with the rest of the Neotropics. *Ecol. Appl.* **30**, e02004 (2020).
12. Sophie, F. *et al.* Data from 'Hyperdominance in Amazonian forest carbon cycling Amazon'. ForestPlots.net https://doi.org/10.5521/ForestPlots.net/2015_1 (2015).
13. Fauset, S. *et al.* Hyperdominance in Amazonian forest carbon cycling. *Nat. Commun.* **6**, 6857 (2015).
14. Williams, M. *et al.* Carbon sequestration and biodiversity of re-growing miombo woodlands in Mozambique. *For. Ecol. Manage.* **254**, 145–155 (2008).
15. McNicol, I. M., Ryan, C. M. & Williams, M. How resilient are African woodlands to disturbance from shifting cultivation? *Ecol. Appl.* **25**, 2320–2336 (2015).

16. Kalaba, F. K., Quinn, C. H., Dougill, A. J. & Vinya, R. Floristic composition, species diversity and carbon storage in charcoal and agriculture fallows and management implications in Miombo woodlands of Zambia. *For. Ecol. Manage.* **304**, 99–109 (2013).
17. Pan, Y. *et al.* A large and persistent carbon sink in the world's forests. *Science* **333**, 988–993 (2011).
18. Tuanmu, M.-N. & Jetz, W. A global 1-km consensus land-cover product for biodiversity and ecosystem modelling. *Glob. Ecol. Biogeogr.* **23**, 1031–1045 (2014).
19. Breiman, L. Random Forests. *Mach. Learn.* **45**, 5–32 (2001).
20. Tramontana, G., Ichii, K., Camps-Valls, G., Tomelleri, E. & Papale, D. Uncertainty analysis of gross primary production upscaling using Random Forests, remote sensing and eddy covariance data. *Remote Sens. Environ.* **168**, 360–373 (2015).
21. Zeng, J. *et al.* Global terrestrial carbon fluxes of 1999-2019 estimated by upscaling eddy covariance data with a random forest. *Sci. Data* **7**, 313 (2020).
22. Xie, M. *et al.* Monitoring of carbon-water fluxes at Eurasian meteorological stations using random forest and remote sensing. *Sci. Data* **10**, 587 (2023).
23. Jung, M. *et al.* Scaling carbon fluxes from eddy covariance sites to globe: synthesis and evaluation of the FLUXCOM approach. *Biogeosciences* **17**, 1343–1365 (2020).
24. Tramontana, G. *et al.* Predicting carbon dioxide and energy fluxes across global FLUXNET sites with regression algorithms. *Biogeosci. Discuss.* 1–33 (2016).
25. Besnard, S. *et al.* Global Age Mapping Integration (GAMI). GFZ Data Services https://doi.org/10.5880/GFZ.1.4.2023.006 (2024).
26. Besnard, S. *et al.* Quantifying the effect of forest age in annual net forest carbon balance. *Environ. Res. Lett.* **13**, 124018 (2018).
27. Houghton, R. A. *et al.* Carbon emissions from land use and land-cover change. *Biogeosciences* **9**, 5125–5142 (2012).
28. Harris, N. L. *et al.* Baseline map of carbon emissions from deforestation in tropical regions. *Science* **336**, 1573–1576 (2012).
29. Stephens, B. B. *et al.* Weak northern and strong tropical land carbon uptake from vertical

profiles of atmospheric CO2. *Science* **316**, 1732–1735 (2007).

30. Gaubert, B. *et al.* Global atmospheric CO_2 inverse models converging on neutral tropical land exchange, but disagreeing on fossil fuel and atmospheric growth rate. *Biogeosciences* **16**, 117–134 (2019).
31. Howard, E. A., Gower, S. T., Foley, J. A. & Kucharik, C. J. Effects of logging on carbon dynamics of a jack pine forest in Saskatchewan, Canada: LOGGED JACK PINE CHRONOSEQUENCE C DYNAMICS. *Glob. Chang. Biol.* **10**, 1267–1284 (2004).
32. Mkhabela, M. S. *et al.* Comparison of carbon dynamics and water use efficiency following fire and harvesting in Canadian boreal forests. *Agric. For. Meteorol.* **149**, 783–794 (2009).
33. Kolari, P. *et al.* Carbon balance of different aged Scots pine forests in Southern Finland: CARBON BALANCE IN BOREAL SCOTS PINE FORESTS. *Glob. Chang. Biol.* **10**, 1106–1119 (2004).
34. Magnani, F. *et al.* The human footprint in the carbon cycle of temperate and boreal forests. *Nature* **447**, 848–850 (2007).
35. Luyssaert, S. *et al.* Old-growth forests as global carbon sinks. *Nature* **455**, 213–215 (2008).
36. Wirth, C., Czimczik, C. I. & Schulze, E.-D. Beyond annual budgets: carbon flux at different temporal scales in fire-prone Siberian Scots pine forests. *Tellus B Chem. Phys. Meteorol.* **54**, 611 (2002).
37. Law, B. E., Sun, O. J., Campbell, J., Van Tuyl, S. & Thornton, P. E. Changes in carbon storage and fluxes in a chronosequence of ponderosa pine: CHANGES IN CARBON STORAGE. *Glob. Chang. Biol.* **9**, 510–524 (2003).
38. Noormets, A., Chen, J. & Crow, T. R. Age-dependent changes in ecosystem carbon fluxes in managed forests in northern Wisconsin, USA. *Ecosystems* **10**, 187–203 (2007).
39. Desai, A. R., Bolstad, P. V., Cook, B. D., Davis, K. J. & Carey, E. V. Comparing net ecosystem exchange of carbon dioxide between an old-growth and mature forest in the upper Midwest, USA. *Agric. For. Meteorol.* **128**, 33–55 (2005).
40. Noormets, A. *et al.* Drought during canopy development has lasting effect on annual carbon balance in a deciduous temperate forest. *New Phytol.* **179**, 818–828 (2008).

41. Gough, C. M., Vogel, C. S., Schmid, H. P., Su, H.-B. & Curtis, P. S. Multi-year convergence of biometric and meteorological estimates of forest carbon storage. *Agric. For. Meteorol.* **148**, 158–170 (2008).